OPTICS

Plug-and-play fiber-optic sensors based on engineered cells for neurochemical monitoring at high specificity in freely moving animals

Bingqian Zhou[1]†, Kuikui Fan[1]†, Jingjing Guo[2]†, Jiesi Feng[3], Changxi Yang[1], Yulong Li[3], Songhai Shi[4,5], Lingjie Kong[1,5]*

In vivo detection of neurochemicals, including neurotransmitters and neuromodulators, is critical for both understanding brain mechanisms and diagnosing brain diseases. However, few sensors are competent in monitoring neurochemical dynamics in vivo at high specificity. Here, we propose the fiber-optic probes based on engineered cells (FOPECs) for plug-and-play, real-time detection of neurochemicals in freely moving animals. Taking advantages of life-evolved neurochemical receptors as key components, the chemical specificity of FOPECs is unprecedented. We demonstrate the applications of FOPECs in real-time monitoring of neurochemical dynamics under various physiology and pathology conditions. With no requirement of viral infection in advance and no dependence on animal species, FOPECs can be widely adopted in vertebrates, such as mice, rats, rabbits, and chickens. Moreover, FOPECs can be used to monitor drug metabolisms in vivo. We demonstrated the neurochemical monitoring in blood circulation systems in vivo. We expect that FOPECs will benefit not only neuroscience study but also drug discovery.

INTRODUCTION

Neurotransmitters and neuromodulators play important roles in a wide variety of physiological and pathological processes. As endogenous chemicals, they relay signals to specific neuronal synapses or assist in regulating the effects of transmitting information crucial for the regulation of normal physiological functions such as sleep, movement, and cognition (*1*). Moreover, abnormal neurochemical signals indicate the onset of several diseases, including Parkinson's disease (PD), Alzheimer's disease, epilepsy, and depression (*2*–*4*). Thus, the in vivo detection of neurochemical dynamics at high sensitivity and high specificity is highly desired in understanding brain functions, diagnosing brain diseases, and prompting drug discoveries.

However, conventional detection methods fail in monitoring these neurochemicals selectively and sensitively in vivo. Although microdialysis can accurately identify the extracellular concentration of neurochemicals in vivo (*5*, *6*), it is of low temporal resolution (>10 min per sample) and the sampling procedures are complex (*7*, *8*). Electrochemical detection techniques are of high temporal resolutions and high sensitivity (*9*, *10*). For example, on the basis of fast-scan cyclic voltammetry, NeuroString (*11*) was developed to detect neurotransmitters in the brain and guts. However, it is not competent in distinguishing neurochemicals of similar chemical structures, such as dopamine (DA) and norepinephrine (NE) (*12*, *13*). To improve the chemical specificity, efforts have been made to integrate aptamer-based recognition elements into organic transistors, such as organic electrochemical transistors and electrolyte-gate organic field-effect transistors (*14*–*18*). However, because of the inherent disadvantages of electrochemical strategies, the disturbance of normal brain activity in applying extra voltage during sensing becomes a big concern (*19*). Moreover, all electrochemical strategies are susceptible to electromagnetic interference.

Recently, fluorescence protein–based sensors have been developed to monitor neurochemical dynamics in vivo. For example, cell-based fluorescently engineered receptors for neurotransmitters (CNiFERs) were developed for volumetric signaling of neurotransmitters, which convert extracellular neurotransmitter signals into intracellular calcium signals and report [Ca^{2+}] with a genetically encoded fluorescent Ca^{2+} sensor (*20*, *21*). Unfortunately, as CNiFERs signals were detected by two-photon fluorescence imaging of implanted cells, sensitive sensing can only be achieved in superficial layers of the cerebral cortex, limited by the bottleneck of imaging depth. So far, no demonstrations of CNiFERs have been achieved in sensing neurotransmitters in deep brains, which, however, are origins and/or targets of most neurotransmitters. Besides, G protein–coupled receptor activation–based (GRAB) neurotransmitter sensors and others (e.g., dLight) were developed to detect neurochemical dynamics directly in vivo (*22*–*27*). After viral infections, fluorescent GRAB neurotransmitter sensors are expressed on cell membranes to indicate neurotransmitters at fast kinetics, ultrahigh spatiotemporal resolution, and super specificity. However, the time cost of viral infection generally takes ~2 weeks (*28*), and even worse, it will be much longer if one plans to cultivate transgenic animals, considering the reproductive cycle of model animals. Moreover, for different animal species, laborious work is needed to explore strategies for efficient viral infection (*29*), as their specific gene codes of neurotransmitter receptors may be different. On the other hand, it is difficult, if possible, to monitor

[1]State Key Laboratory of Precision Measurement Technology and Instruments, Department of Precision Instruments, Tsinghua University, Beijing 100084, China. [2]School of Instrumentation and Optoelectronic Engineering, Beihang University, Beijing 100191, China. [3]State Key Laboratory of Membrane Biology, School of Life Sciences, Peking University, Beijing 100871, China. [4]Tsinghua-Peking Joint Center for Life Sciences, Beijing Frontier Research Center of Biological Structures, School of Life Sciences, Tsinghua University, Beijing 100084, China. [5]IDG/McGovern Institute for Brain Research, Tsinghua University, Beijing 100084, China.
*Corresponding author. Email: konglj@tsinghua.edu.cn
†These authors contributed equally to this work.

neurochemical dynamics in blood circulation system in vivo with current fluorescence protein sensors. Crucially, the above methods would be very difficult (or even impossible) to implement in humans.

Here, we propose fiber-optic probes based on engineered cells (FOPECs) for plug-and-play, real-time monitoring of neurochemicals at high specificity in freely moving animals. As "plug-and-play" probes, FOPECs can function once implanted in wild-type animals without time-consuming and complex procedures of cultivating transgenic model organisms or transfecting with engineered viruses. We integrate genetically engineered cells that express GRAB neurotransmitter sensors with optical fibers for real-time sensing, which can not only skip the time-consuming procedures of viral infection but also ensure high specificity. Specifically, we embed these engineered cells in biocompatible hydrogels and load the mixtures around the tips of optical fibers for sensing. We verify the performance of FOPECs by real-time sensing of NE, DA, and adenosine triphosphate (ATP) under various physiological and pathological conditions in the brains of mice and rats in vivo. In addition, to demonstrate the general applicability of our technique in sensing neurotransmitters in vertebrates, we implant FOPECs into the venous vessels of rabbits to detect the drug-induced elevation of DA. FOPECs provide a novel platform for monitoring neurochemical dynamics in vivo, promising for neuroscience study and drug discovery.

RESULTS

Characterization of FOPECs in vitro and in vivo

The schematic diagram for monitoring neurochemical dynamics with FOPECs is shown in Fig. 1. In FOPECs, sensing cells are embedded in biocompatible hydrogels and loaded around the tips of optical fibers. The hydrogels have a porous structure that enables rapid diffusion of small analytes into the polymeric networks, while large molecules comparable or larger than the pore size will be physically entrapped (*30*). Considering that neurochemicals are small molecules that can freely pass through the hydrogel matrix, there are ample opportunities for sensing cells to contact with neurochemical molecules in the microenvironments (*31*, *32*). To protect sensing cells and secure the connection between the optical fiber and hydrogel, we encapsulate the fiber tips and hydrogels in glass capillaries (see Materials and Methods and fig. S1 for details). Besides, to facilitate cell injection and reduce the capillary effect, rectangular windows are fabricated at the front end of the capillaries by laser cutting. For self-reference measurement, we use engineered cells expressing two fluorescent proteins simultaneously, transfected with GRAB plasmids such as pDisplay-$GRAB_{NE2h}$-IRES-mCherry-CAAX. The green fluorescent protein (GFP) is tagged on GRAB neurotransmitter sensors (such as $GRAB_{NE2h}$) for signaling. The red fluorescent protein (RFP; such as mCherry) is used for reference, as it is not sensitive to neurotransmitters and its fluorescence signal experiences the same perturbations as that of GFP.

We transfect human embryonic kidney (HEK) 293T cells with plasmids (table S1) that express GRAB neurotransmitter sensors and embed them in Matrigel for three-dimensional (3D) culture. Then, we characterize sensing performance of FOPECs in vitro by confocal imaging. Taking the NE-sensitive FOPECs, of engineered cells expressing $GRAB_{NE2h}$, as an example (Fig. 2, A to C, and fig. S2), after adding 100 μM NE, the fluorescence signal of GFP is enhanced by about 67.6%, while the reference signal of RFP is almost unchanged (less than 0.4%). The ratio of the fluorescence increases to its initial value ($\Delta F/F_0$) is used to indicate changes of neurotransmitter concentrations. The gradient concentration responses of NE-sensitive FOPECs span from 100 nM to 100 μM (Fig. 2D). The rising time (τ_{on}) is about 17.4 s by adding 100 μM NE solution

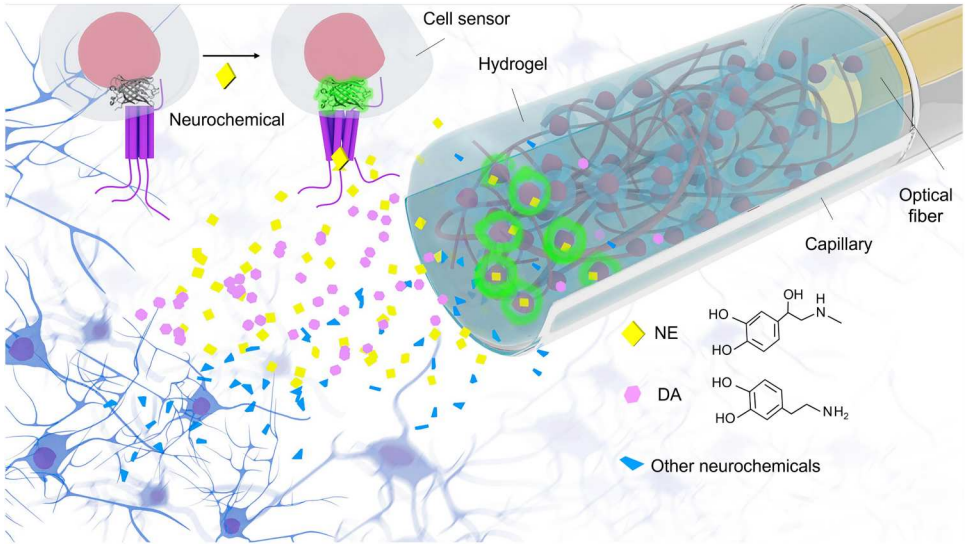

Fig. 1. Schematic diagram of neurochemical sensing in vivo with FOPECs. FOPECs are implanted in the animal brains to measure neurochemical dynamics. The engineered cells are loaded around the tips of optical fibers, and glass capillaries are used to protect the cells from loss and leakage during implantation. Rectangular windows are fabricated at the front end of the capillaries by laser cutting to facilitate cell injection and reduce the capillary effect. Inset at the upper left: principle of neurochemical sensing with engineered cells. Once neurochemicals are detected, fluorescence signals of GRAB neurotransmitter sensors are enhanced. NE, norepinephrine; DA, dopamine.

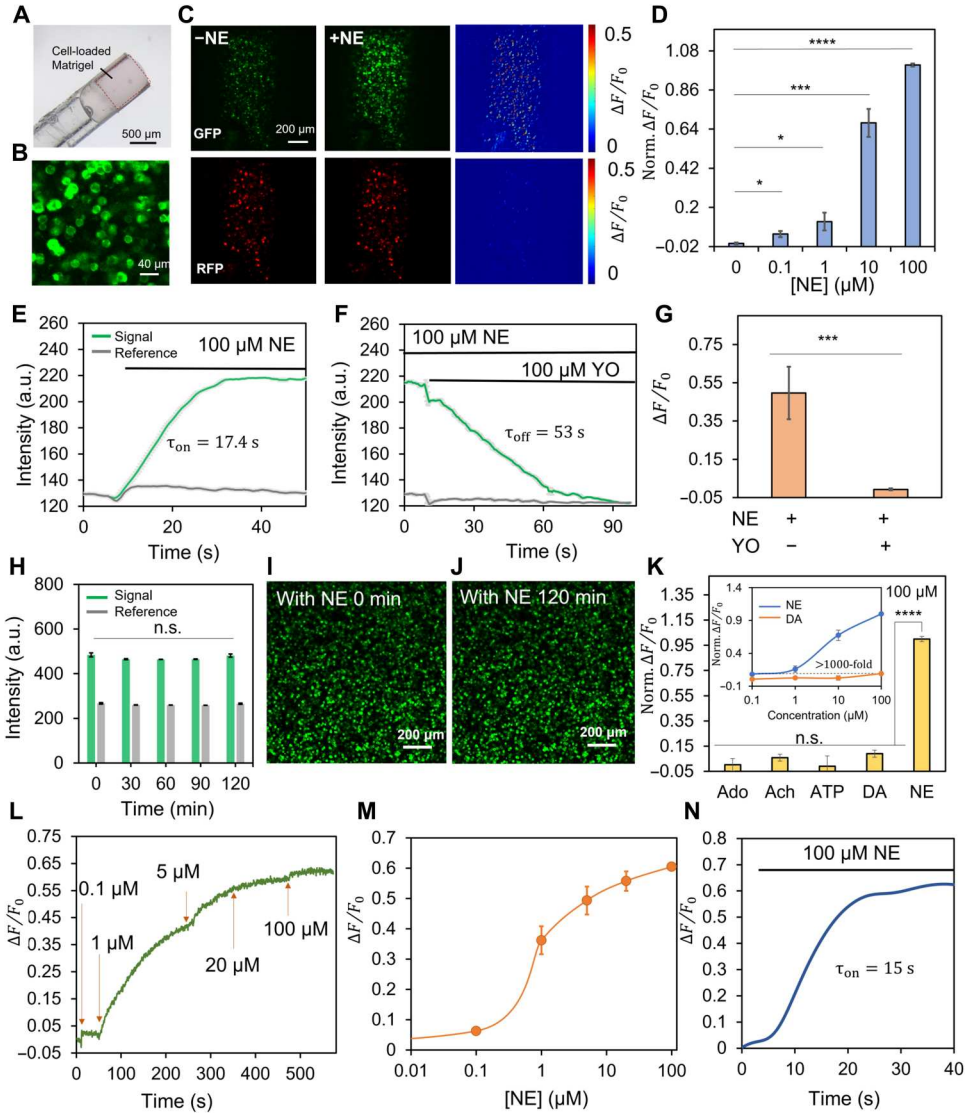

Fig. 2. Performance characterization of NE-sensitive FOPECs in vitro. (**A**) Photo of a NE-sensitive FOPEC. The region of the cell-loaded Matrigel is indicated by red dotted lines. (**B**) Fluorescence image of engineered HEK293T cells in Matrigel under 488-nm excitation. (**C**) Example of photometric-based cell sensing, showing the signal (top) and reference (bottom) fluorescence response of HEK293T cells in Matrigel to 100 μM NE. GFP, green fluorescence protein; RFP, red fluorescence protein. $\Delta F/F_0$ denotes the ratio of the increase of fluorescence intensity to its initial value. (**D**) Response of NE-sensitive FOPECs to various NE concentrations ($n = 3$). (**E**) Rising time response (τ_{on}) of NE-sensitive FOPECs under 100 μM NE ($n = 3$). (**F**) Descent time response (τ_{off}) of NE-sensitive FOPECs under 100 μM YO ($n = 3$). (**G**) Fluorescence changes of NE-sensitive FOPECs in response to 100 μM NE and 100 μM YO ($n = 3$). (**H** to **J**) Stability of NE-sensitive FOPECs under 100 μM NE for 120 min ($n = 3$). Initial fluorescence image (I) and fluorescence image after 120 min (J). (**K**) Specific response of NE-sensitive FOPECs ($n = 3$). The concentration of each drug is 100 μM. The inset image shows the specific response of NE-sensitive FOPECs, differentiating between NE and DA ($n = 3$). (**L** to **N**) Characterization of NE-sensitive FOPECs under custom-made optical sensing setup. (L) Fluorescence changes of the probe at different concentrations of NE. (M) Gradient response curve of NE-sensitive FOPECs ($n = 3$). (N) Response curve of NE-sensitive FOPECs under 100 μM NE solution. Unless noted, values with error bars indicate means ± SEM. HEK293T cells are transfected with plasmids that express $GRAB_{NE2h}$. The length of the cell-hydrogel mixture in (E) to (G) and (L) to (N) is 0.25 mm. n.s. denotes $P > 0.05$, *$0.01 < P < 0.05$, ***$P < 0.001$, ****$P < 0.0001$ (Student's t test). a.u., arbitrary units.

(Fig. 2E), and the decline time (τ_{off}) is about 53 s by adding 100 μM α2-adrenergic receptor antagonist yohimbine (YO) solution (Fig. 2F). The rapid decrease of fluorescence signal after adding YO indicates that the fluorescence change is the result of the binding between NE molecules with the receptor proteins expressed by the engineered HEK293T cells (Fig. 2G). No desensitization is observed for up to 2 hours under 100 μM NE solution (Fig. 2, H to J). Besides, we show the chemical specificity of NE-sensitive FOPECs in Fig. 2K, which suggests that FOPECs can distinguish structurally similar neurotransmitters, such as NE and DA [more than 1000-fold affinity (*22*)]. The in vitro characterizations of DA-sensitive FOPECs (fig. S3) and ATP-sensitive FOPECs (fig. S4) are consistent with those of NE-sensitive FOPECs, which paves the way for in vivo sensing at high specificity.

We test the gradient response and response time of NE-sensitive FOPECs using a custom-made optical setup (fig. S5). Two fiber-

coupled lasers at 473 and 561 nm are launched into FOPECs through multimode fibers (MMFs) and used as the excitation sources for GFP and RFP, respectively. Both the red and green fluorescence are collected by the MMF and guided to a dichroic beam splitter, which splits the red and green signals onto two avalanche photodiodes (APDs). For weak signal detection, we use a lock-in amplifier to improve the signal-to-noise ratio (SNR). Notably, the probe shows highly sensitive responsiveness in micromolar concentrations of NE, spanning the physiologically relevant concentrations (Fig. 2, L and M). The rising time (τ_{on}) is about 15 s at 100 μM NE solution (Fig. 2N), which is consistent with previous results in Fig. 2E based on imaging.

To further improve the sensing ability of FOPECs, we mainly optimize the excitation power, volume/length, and cell density of the loaded cell-hydrogel mixture (Fig. 3). It is found that there is a threshold (20 μW) of excitation power (Fig. 3A), above which the detected signal is less affected by the excitation power. We choose 20 μW as the optimal excitation power considering both the fluorescence increment and the bleaching of photosensitive proteins. The neurotransmitter detection of FOPECs relies on the passive diffusion of analytes into the hydrogel matrices driven by the concentration gradient. Thus, the volume of the cell-hydrogel mixtures, proportional to the length along the fiber axis (defined as L), affects the sensitivity and response time of the sensors (Fig. 3, B to D, and fig. S6). We experimentally characterize the fluorescence collection efficiency of FOPECs. As shown in fig. S7, as the excitation laser spreads out the fiber, a conical shape can be observed due to absorption and scattering of the medium, and the optically sampled length is optimized at 500 μm. To balance response time and signal strength, we choose L = 0.5 mm in the following experiments (Fig. 3, E to G). In addition, the dependence of the state of HEK293T cells on cell density in Matrigel is further examined by

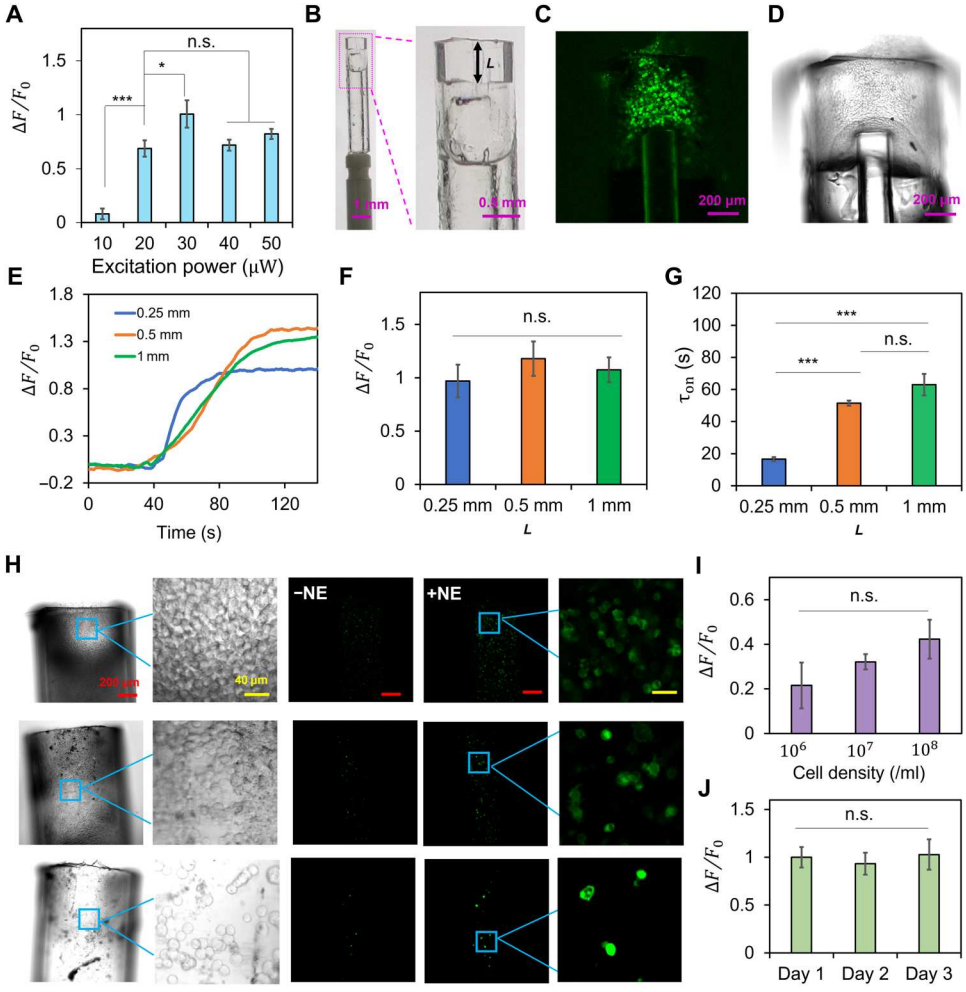

Fig. 3. Performance optimization of FOPECs in vitro. (**A**) Threshold of excitation light (470 nm) power for NE-sensitive FOPEC sensing. Fluorescence response to 100 μM NE at different excitation light powers (n = 3). (**B** to **D**) Photos of NE-sensitive FOPECs (L = 0.5 mm). Photos of the probe before loading cells are shown in (B). Confocal images of the probe after loading cells are shown in (C) and (D). (**E** to **G**) Sensing performance of NE-sensitive FOPECs for probes of different L values. Response curves, fluorescence increment, and response time to 100 μM NE are shown in (E), (F), and (G), respectively (n = 3). (**H** and **I**) Dependence of the fluorescence response of FOPECs on cell density, characterized by confocal imaging. (H) Photos, initial fluorescence images, and fluorescence changes for probes of different cell densities (10^8, 10^7, and 10^6 cells/ml from top to bottom rows) in the presence of 10 μM NE. (I) Plot of $\Delta F/F_0$ versus cell density in the presence of 10 μM NE (n = 3). (**J**) Long-term stability of NE-sensitive FOPECs. Fluorescence response to 100 μM NE after FOPEC fabrication (n = 3). Unless noted, values with error bars indicate means ± SEM. HEK293T cells are transfected with plasmids that express $GRAB_{NE2h}$. n.s. denotes $P > 0.05$, *$0.01 < P < 0.05$, ***$P < 0.001$ (Student's t test).

confocal imaging (Fig. 3, H and I, and figs. S8 and S9). We find that cell density between 10^7 and 10^8 cells/ml is most suitable, providing relatively strong signals. Furthermore, FOPECs of such cell density can be stored in cell incubators for many days with no degraded performance (Fig. 3J). On the basis of the above optimization processes, the limit of detection (LOD) of the NE-sensitive FOPECs can reach 24.5 nM [signal-to-noise ratio (S/N) = 3], as shown in fig. S10.

To examine whether FOPECs maintain their sensitivity in vivo, we implant the NE-sensitive FOPECs combined with administration catheters into the ventricle of mouse brains. Under ventricular injection of NE solution, a notable increase of fluorescence signals can be detected with an LOD of about 77 nM, indicating the ability of quantifying neurotransmitters in vivo under physiological and pathological conditions (fig. S11). In addition, we also test the application of FOPECs in different animal models with the ventricular injection of NE solution, where FOPECs are implanted into the third ventricle (3V) of chicken brains, and sensitive response are achieved (fig. S12). To further investigate the long-term biocompatibility of FOPECs, we test the immune response after a week of FOPEC implantation and find no significant inflammation and immune responses (fig. S13).

In vivo neurochemical sensing with FOPECs under physiological conditions

NE plays an important role in processing sensory information, regulating attentional function, and dealing with sleep-wake or wakeful states (*33*). Impaired NE transmission is associated with many neurological diseases, including stress, attention deficit hyperactivity disorder (ADHD) (*34*), and PD (*4*). To probe the NE dynamics in mouse brains in vivo, we implant NE-sensitive FOPECs at hypothalamus, one of the brain areas that release high levels of NE during stress (*35*).

As plug-and-play sensors, FOPECs can be used for real-time sensing immediately after acute implantation in wild-type mice, without the need for viral infection in advance. We test NE dynamics in both the lateral hypothalamus (LH) and the paraventricular nucleus of hypothalamus (PVN) under stressful conditions in freely moving mice (Fig. 4A and fig. S14, G and H). During forced swimming tests, significant increases of fluorescence signal are observed immediately, followed by continuous rising until the mice are removed from the water tank. We test the mice with forced swimming for three times in a session and find that the fluorescence responses in LH are reproducible. In addition, we test signal changes on different days, indicating that the working lifetime of FOPECs is more than 7 days in vivo (Fig. 4B and table S2). A reproducible dynamic trend can still be seen after the implantation of FOPEC for several days, although the signals are not as strong as those on the first day (Fig. 4, B and C). To verify that the signal attenuation is not caused by the behavioral tolerance of the animals themselves, we repeat the above experiments with AAV9-hSyn-$GRAB_{NE2h}$ virus–infected mice. After 2 weeks of viral expression ($GRAB_{NE2h}$) in the LH brain region of mice, we implant optical fibers and detect fluorescence dynamics during forced swimming for seven consecutive days and find that the signal dynamics is almost unchanged (fig. S14, A to F). We further examine the survival rate of cells in the FOPEC and find that the cell death rate gradually increases within a week, indicating that the signal attenuation is presumably attributed to cell death (fig. S15). The plateau followed by a decrease toward the baseline after each forced swimming might be a stress-related learning effect (*36*, *37*). A similar plateau effect is observed in wild-type mice after virus transfection (AAV9-hSyn-$GRAB_{NE2h}$) in forced swimming process (fig. S14A). Meanwhile, we find that the NE dynamics stimulated by stress shows large individual differences (fig. S16). Moreover, we compare the NE signals at two locations, LH and PVN, with FOPECs (Fig. 4, D to F) and find that the signal changes are similar, agreeing with the fact that the release of NE is widely distributed in the hypothalamus under stress. These results suggest the promising capability of FOPECs in detecting neurochemical dynamics in physiological states of freely moving animals.

In vivo neurochemical sensing with FOPECs in drug metabolism or under pathological conditions

DA is another central monoamine neurotransmitter that regulates a complex set of processes, including reward signaling, reinforcement learning, and attention (*38*). Abnormal levels of DA are related to neurological disorders, including PD, drug addiction, ADHD, and schizophrenia (*39*). Levodopa (L-dopa), a drug that can treat PD (*40*, *41*), is a prodrug of DA. Once L-dopa is transported across the blood-brain barrier, it is converted into DA by aromatic L-amino acid decarboxylase to exert pharmacological effects. Studies have shown that intraperitoneal injection of L-dopa solution can cause a significant increase of DA in the mouse brain (*42*).

To demonstrate the performance of FOPECs in drug metabolism in vivo, we implant the DA-sensitive FOPECs of cells expressing $GRAB_{DA2h}$ into the hippocampal CA1 region of the brains of wild-type mice (Fig. 5A) and inject L-dopa intraperitoneally. A few minutes later after the injection of L-dopa, the fluorescence signal of DA increases significantly and reaches the highest peak in about 40 min (Fig. 5B). As a control, we inject normal saline intraperitoneally under the same conditions, and no signal changes are detected (Fig. 5C). The time for reaching the highest peak agrees with that in a former report detected by microdialysis (*43*), suggesting the capability of FOPECs in the study of in vivo pharmacology. To verify the specificity of our sensors in vivo, especially in distinguishing DA and NE, we test the NE-sensitive FOPECs and DA-sensitive FOPECs by intraventricular administrations, which suggest excellent discernibility (fig. S17).

Moreover, we demonstrate the application of ATP-sensitive FOPECs of cells expressing $GRAB_{ATP1.0}$ in the study of seizures in vivo. Different from NE and DA, ATP is an energy storage molecule that is ubiquitous in all cell types throughout all organisms (*44*), but its release into extracellular space is found to serve as a kind of purinergic neurotransmitters (*45*). Notably, various acute brain insults, including traumatic brain injury, cerebral ischemia, and seizures (*46*), can trigger a sustained increase in extracellular ATP. Studies have shown that intraperitoneal injection of kainic acid (KA) can cause epileptic seizure in mice, leading to specific discharge and ATP release in the hippocampus of the brains (*47*, *48*). We implant ATP-sensitive FOPECs in the hippocampal CA1 region of mouse brains and monitor the release of ATP in epileptic states induced by KA injection (Fig. 5D). To verify the KA-induced seizures, we also embed an electroencephalography (EEG) device in the hippocampus to record abnormal discharge (fig. S18). Compared with the control group of saline injection, ATP in the hippocampus increased continuously in the KA-induced epileptic seizure group, indicating that the epileptic process is accompanied by the release of a large amount of ATP (Fig. 5, E and F).

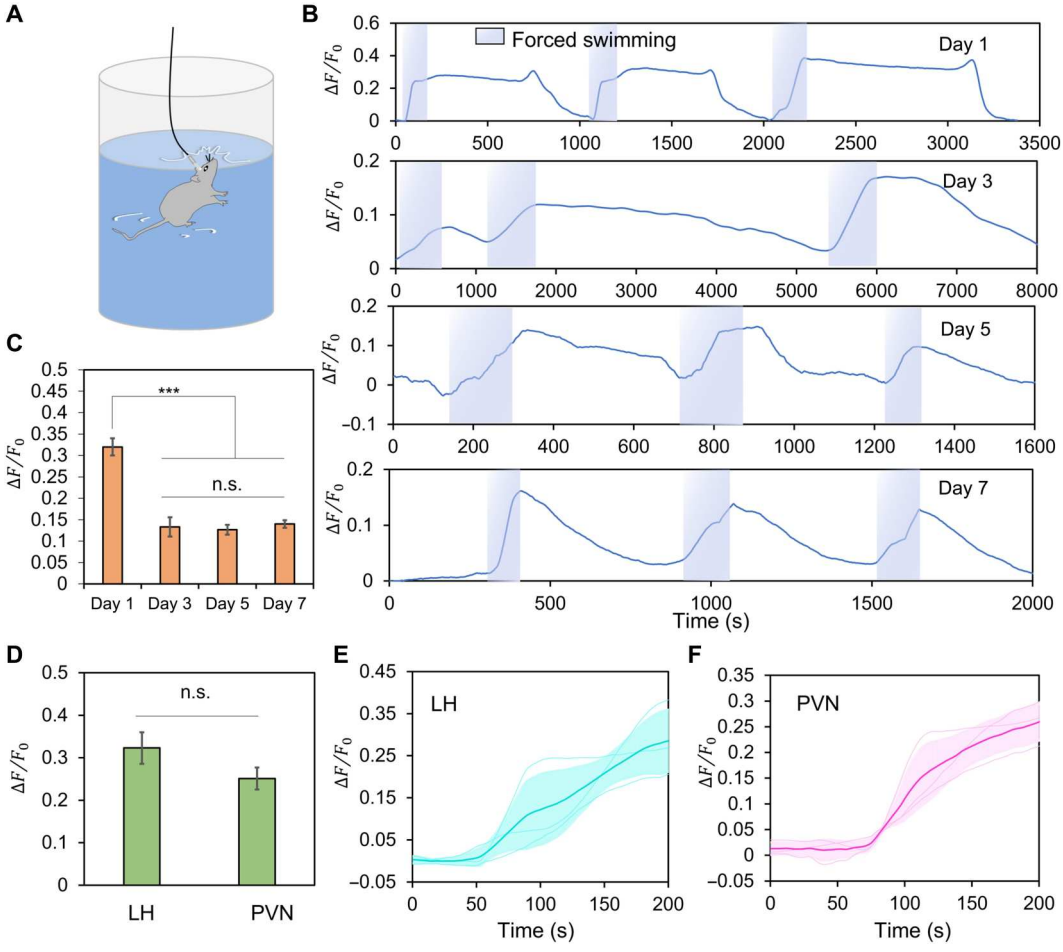

Fig. 4. Real-time monitoring of NE dynamics with FOPECs in different brain regions of freely moving mice under stress conditions. (**A**) Experimental diagram of mouse forced swimming test. (**B**) Representative traces of NE dynamics in the lateral hypothalamus (LH) of mouse brain during the forced swimming test on different days. Mice are forced to swim intermittently three times per session. Areas marked in blue boxes: time period of forced swimming. (**C**) Response of NE-sensitive FOPECs during forced swimming on different days ($n = 3$). (**D**) Statistical data of NE signals from two different brain regions, including LH and paraventricular nucleus of hypothalamus (PVN), during the first session of forced swimming ($n = 3$). (**E** and **F**) NE signals in LH and PVN during forced swimming for the first time ($n = 3$), respectively. Dark solid lines, average results of multiple datasets; light solid lines, data for each mouse; light area, error interval. HEK293T cells are transfected with plasmids that express $GRAB_{NE2h}$. n.s. denotes $P > 0.05$, $^{***}P < 0.001$ (Student's t test).

General applicability of FOPECs in sensing neurochemicals in vertebrates in vivo

Benefiting from the fact that the neurochemical sensing of FOPECs is based on engineered cells inside the probes, FOPECs can be generally applied for plug-and-play sensing in various animal models, with no additional procedures. As an example, we monitor the NE dynamic in rat brains in vivo in response to the intraperitoneal injection of pargyline. Pargyline is an irreversible nonselective monoamine oxidase inhibitor drug mainly used for the treatment of severe hypertension (*49*). We implant NE-sensitive FOPECs into the LH region of rat brains and detect the dynamics of NE (Fig. 5G) after intraperitoneal injection of pargyline. As shown in Fig. 5 (H and I), a sustained rise of NE fluorescence signal is observed correspondingly.

In addition to detecting neurochemical dynamics in the brains in vivo, it is also of great significance to monitor the dynamic levels of neurochemicals in flowing vasculatures in clinical medicine in vivo. We first verify the capability of NE-sensitive FOPECs in detecting NE in fresh blood in vitro. By adding NE of different concentrations to mouse blood samples, we record fluorescence increments. As shown in fig. S19, our probes can detect signals sensitively without interferences from other elements in blood plasma. We then demonstrate the application of modified DA-sensitive FOPECs in monitoring DA in the auricular vein of rabbits after intraperitoneally injecting L-dopa (Fig. 5J and fig. S20A). The vein vessels of rabbit ear are chosen for blood detection in vivo, considering that their adequate diameters allow for easy surgical access and implantation. As shown in Fig. 5 (K and L), the signals of DA-sensitive FOPECs in the flowing blood of rabbits increase after the injection of L-dopa, correspondingly. Besides, 1 hour after L-dopa administration, we immediately take out blood samples (fig. S20B) and detect the DA signals with FOPECs in vitro. In comparison, the results are similar, suggesting the robustness of FOPECs in detecting neurochemicals in flowing vasculatures in vivo.

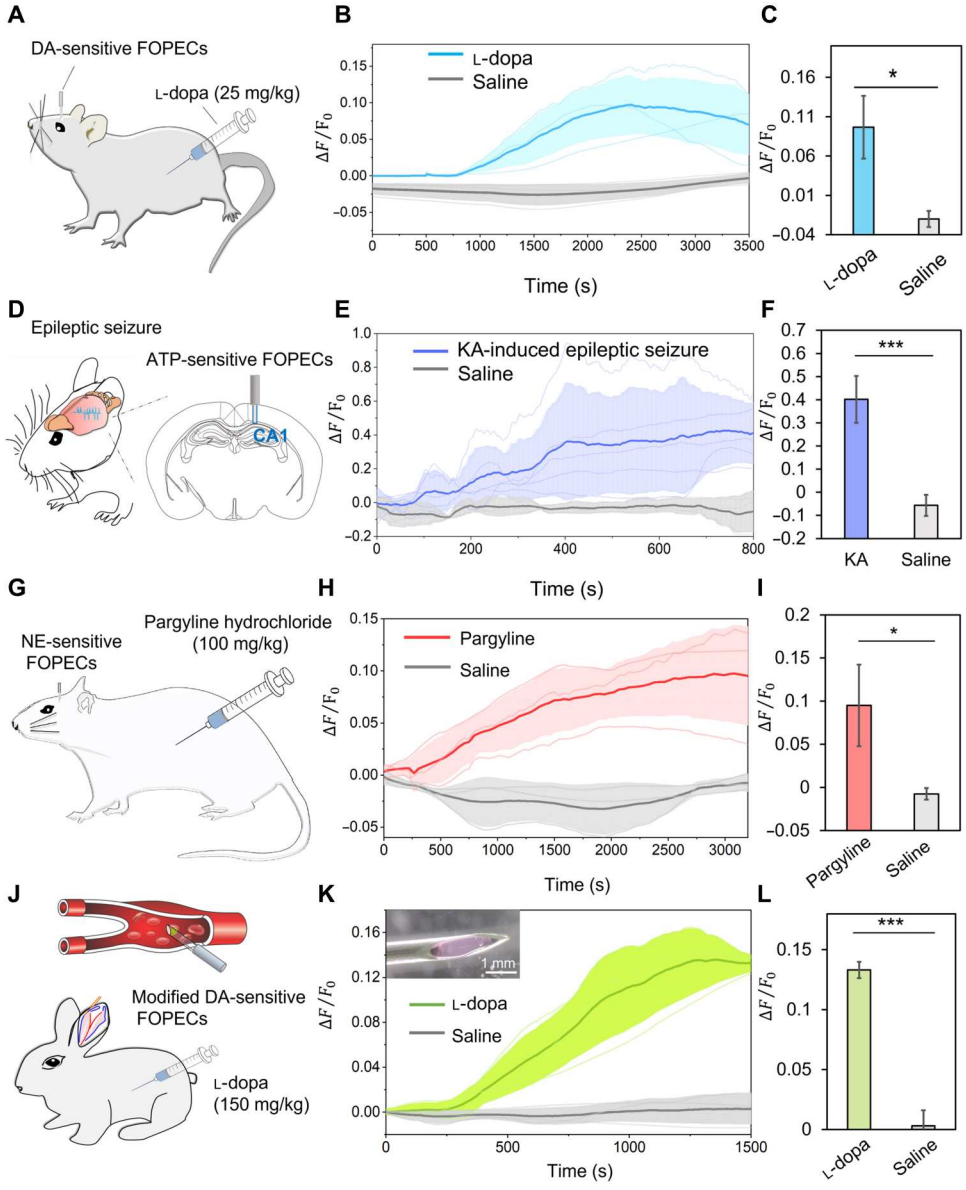

Fig. 5. Real-time monitoring of neurochemicals with FOPECs in drug metabolism and under pathological conditions in various animals and various organs in vivo. (**A**) Experimental diagram of mice under drug (L-dopa) administration. (**B**) DA dynamics detected with DA-sensitive FOPECs in the hippocampus of mouse brains in vivo after L-dopa or saline is injected intraperitoneally ($n = 3$). (**C**) Maximum fluorescence increments due to L-dopa and saline. *$P < 0.05$ (Student's t test). (**D**) Experimental diagram of KA-induced epileptic seizure in mice. (**E**) Fluorescence dynamics of ATP-sensitive FOPECs in the hippocampal CA1 after intraperitoneal injection of KA or saline ($n = 5$). (**F**) Maximum fluorescence increments due to KA and saline. ***$P < 0.001$ (Student's t test). (**G**) Schematic diagram of NE sensing in rat brains in vivo after intraperitoneal injection of pargyline. (**H**) Fluorescence dynamics of NE-sensitive FOPECs in the LH of rat brains after intraperitoneal injection of pargyline or saline ($n = 3$). (**I**) Maximum fluorescence increments due to pargyline and saline administration. *$P < 0.05$ (Student's t test). (**J**) Schematic diagram of DA sensing in the auricular vein of rabbits in vivo after intraperitoneal injection of L-dopa. (**K**) Fluorescence dynamics of DA-sensitive FOPECs after intraperitoneal injection of L-dopa or saline ($n = 3$). The inset shows the photo of a modified FOPEC for implanting into the blood vessel of rabbits. (**L**) Maximum fluorescence increments due to L-dopa and saline administration. *$P < 0.05$ (Student's t test). Legends for (B), (E), (H), and (K): Dark solid lines, average results of multiple datasets; light solid lines, data for each mouse; light area, error interval.

DISCUSSION

In conclusion, we propose the novel plug-and-play FOPECs for monitoring neurochemicals at high chemical specificity in freely moving animals. We demonstrate the detection of several neurochemicals, as examples, in vitro and verify the fast time response and high sensitivity of FOPECs. Moreover, we demonstrate the in vivo monitoring of various neurochemicals in the brains under both physiological and pathological conditions and during drug metabolisms. In table S3, we compare FOPECs with current mainstream neurotransmitter sensors. It can be seen that our FOPECs exhibit excellent comprehensive performances, including high specificity, low detection limit, and wide dynamic range. Different from

sensing techniques based on fluorescence sensors (*23*) with viral infection in advance and transgenic breeding, our method can save a lot of time and avoid complex procedures in sample preparation. After acute implantation of FOPECs, we can monitor the neurotransmitter dynamics immediately. Moreover, the sensing performances of FOPECs can be maintained for several days. For potential applications in human, it is much easier and securer to implement FOPECs in humans upon ethical approval compared to fluorescence sensing by gene manipulation.

Another significant advantage of FOPECs is the general applicability for neurochemical sensing in various animal species and various organs in vivo. We successfully demonstrate the applications of neurochemical-sensitive FOPECs in various animal models, including mice, rats, chicken, and rabbits. Besides, we monitor drug-induced DA dynamics in the blood vasculature of rabbits in vivo, which is the first demonstration of monitoring neurochemicals in circulating blood in situ and in real time.

The response rate of FOPECs in the current study is diffusion limited, considering the dynamic equilibrium process between the molecular concentration inside and outside hydrogel networks. The sensor response can be sped up by reducing the volume or length of the cell-loaded hydrogel to decrease the diffusion time required to reach equilibrium. However, reducing the length of cell-loaded hydrogel leads to the decrease of fluorescence signals and SNR. Therefore, there is a trade-off between the response rate and SNR. To further improve the performance of FOPECs, future efforts in fluorescent protein engineering are expected to improve the sensor brightness and affinity.

Besides, FOPECs can be further improved to be less invasive, more biocompatible, and easily replaceable. The capillaries in current FOPECs are made of glass materials that have a Young′s modulus ($E \approx 10$ GPa) at least five orders of magnitudes higher than that of the soft brain tissues [typically 1 to 100 kPa (*50*)]. The mechanical mismatch may lead to injuries of host tissues during vigorous tissue movements. For future improvement, capillaries made of soft and biocompatible materials such as silicones can be used. Moreover, for long-term monitoring, pluggable fixation protocols should be developed to replace the degraded probes.

FOPECs can be used for sensing various chemicals in vivo with specific engineered cells, not limited to the cells with GRAB or CNiFERs indicators. We expect broad applications of FOPECs in monitoring neurochemical dynamics in vivo for neuroscience study, disease monitoring, and drug discovery.

MATERIALS AND METHODS

Cell culture and transfection

HEK293T cells (American Type Culture Collection cell line CRL-3216) are cultured at 37°C in 5% CO_2 in Dulbecco′s modified Eagle′s medium (DMEM; Gibco) supplemented with 10% (v/v) fetal bovine serum (FBS; Gibco) and 1% (v/v) penicillin-streptomycin (P/S; Gibco). Transfection of HEK293T cells can express G protein–coupled receptor. HEK293T cells are transfected on the basis of artificial liposome method (with a typical ratio of 1 μg of plasmids to 3 μg of liposomes). The culture medium (DMEM + 10% FBS) needs to be changed without P/S 1 day before transfection. When the cell density reaches 70 to 80%, plasmids and liposomes are added to the medium (Opti-MEM, serum-free, Gibco). Fifteen microliters of plasmids and 45 μl of liposomes are added into 400 μl of medium, respectively (Opti-MEM, serum-free, Gibco); this mixture is shaken gently and let stand for 5 min. Liposome solution is added dropwise into the plasmid solution, shaken gently, and let stand for 20 min. The mixed solution is slowly added dropwise into the 100-mm-diameter petri dish full of cells (430591, Corning). The medium (DMEM + 10% FBS + 1% P/S) is changed about 6 hours after transfection. Generally, after 24 hours, the transfected cells can fully express fluorescent protein receptors. The GRAB indicators expressed on different neurochemical sensors are shown in table S1.

Animal husbandries

C57/BL6 wild-type male mice (8 to 9 weeks old) and Sprague-Dawley male rats (8 to 10 weeks old) are obtained from Charles River Laboratories (Beijing, China); New Zealand rabbit (~3 kg) and little chick (1 month old) are separately obtained from Fangyuanyuan farm and Zhaoqiang farm (Beijing, China). Those animals are maintained in a temperature-controlled room on a 12-hour light/dark cycle (lights on 06:00 to 18:00) with ad libitum access to food and water and fed a standard diet. All procedures for animal surgery and experimentation are approved by the Institutional Animal Care and Use Committee at the Tsinghua University.

Preparation of FOPECs

Fabrication procedure of FOPECs is mainly divided into four steps (fig. S1). The first step is to fill the glass capillary with ultraviolet (UV) glue (NOA61, Norland) in the portion that does not need to load cells, and the second step is to secure the connection of the fiber optic cannula and capillary under UV radiation. The inner diameter and outer diameter of the glass capillary (BJ-40, Jitian Bio) were 0.8 and 1 mm, respectively. To facilitate cell injection, we use the laser processing technology (*51*) to cut a notch (0.5 mm in depth) at the front end of the capillary, so a rectangular window is formed. The length of the window can be designed as 0.25, 0.5, and 1 mm, according to experimental needs. The fiber optic cannula [ferrule size, 1.25 mm; fiber core diameter, 200 μm; numerical aperture (NA) = 0.37, Inper], which consists of a ceramic ferrule and a length of protruding optical fiber, is used to guide the light. There are two types of fiber optic cannula with different protruding fiber lengths: 5 mm for implantation in any brain region of mice and hippocampus in rats, and 8 mm for implantation into the deep brain regions of rats, such as the LH brain region. The length of the glass capillary is adjusted so as to match with the fiber optic cannula. For example, glass capillary of 5.5-mm length is used for 5-mm fiber optic cannula, and the remaining length of 0.5 mm is for loading cells. Then, the protruding optical fiber is secured into the glass capillary by about 30-s UV radiation, and the fiber optic probe mold is completed and ready for cell loading. The spatial resolution of the sensor is about 1 mm in diameter, depending on the diameter of glass capillaries.

For the cells to be firmly attached to the front end of the optical fiber, we choose hydrogels to culture cells in a 3D environment (*52*, *53*). Matrigel is a gelatinous protein mixture hydrogel derived from mouse tumor cells and used as a 3D cell culture substrate in vitro (*54*). The most desirable cell type of GRAB sensors used for in vitro detection is HEK293T cells transfected with plasmids, and Matrigel is also suitable for their 3D culture. In the third step, the mixtures of cells and hydrogels are injected into the capillary. About 24 hours after transfection, the induced cells are digested with trypsin to

obtain a cell suspension and then centrifuged to obtain a high-concentration cell suspension (10^6 to 10^8 cells/ml); the cell suspension is mixed with Matrigel at a volume ratio of 1:3. Typically, the number of cells loaded per probe is approximately 3.9×10^6 to 3.9×10^7.

The fourth step is to solidify the cell-loaded hydrogel solution. FOPECs are placed in a cell incubator for ~5 min until HEK293T cells are firmly immobilized in Matrigel, and then the medium constantly supplying nutrients to cells is added for preservation of FOPECs. Since FOPECs are cellular sensors, the storage environment needs to be suitable for cell survival and growth. The prepared probe mold is typically fixed on the bottom of a 35-mm-diameter petri dish (430588, Corning) before being injected with cells and is sterilized by UV light for 30 min. The process of injecting cells should also be performed in a sterile environment. Last, the probe is kept in the petri dish of medium (DMEM + 10% FBS + 1% P/S) for long-term preservation. This preservation method can make the cells survive for at least 1 week, and the medium (DMEM + 10% FBS + 1% P/S) is changed every 2 days.

In vivo implantation

All surgical tools are sterilized in an autoclave before surgery. Mice are anesthetized with isoflurane: 4% (v/v) for induction, 1.5 to 2.0% (v/v) (mice and little chicken), and 2.5 to 3.5% (v/v) (rats) for maintenance; the mouse body temperature is maintained at 37°C using heating pad. The eyes are covered with ophthalmic ointment to prevent drying, the mouse is mounted in a stereotaxic frame with ear bars, and a surgical area is cleared with electric shave. We first use a scalpel blade to cut and remove the skin over the skull surface and remove the periosteum to expose and clean the surface of the skull. An empty glass pipette is lowered to the bregma, and the antero-posterior and medio-lateral coordinates are recorded to complete the calibration process. Referring to the mouse brain atlas, we calculate the position of the implantation site. Next, we open a 1.5 mm–by–1.5 mm diameter aperture on the skull using miniature handheld skull drill (68605, RWD Life Science). Then, a cylindrical cone pin (A4000810, Brand) is gradually inserted to create an opening and channel at uniform speed. Furthermore, the blood stains are cleaned with phosphate-buffered saline (PBS) buffer and a 21-gauge needle connected to a vacuum pump is used to remove dirt, ensuring that the passageway is unblocked and clean after reaching the desired depth. Sponge is placed on the window to keep it moist while preparing to implant the biosensor. The biosensor is moved to the target X and Y coordinates, lowered, and continued to below the skull surface until it is in the target areas. After completing biosensor implantations, the thinned-skull window is rinsed with PBS, and we wait for the skull to dry. Then, the site is sealed with dental cement (mix carbon toner). We cover the rest of the skull surface, ensuring that the edges of the skin are covered by cement, and we let it dry for 20 min. Following the surgery, isoflurane administration is stopped and the mouse is left in a cage until it fully recovers from anesthesia. We inject 5% (w/v) glucose in saline (subcutaneously) for rehydration and buprenorphine (0.05 to 0.1 mg/kg, intraperitoneally, instant release) for post-operative analgesia. To minimize potential immunological reaction, the mice are injected daily with cyclosporine (20 μl/100 g, intraperitoneally) starting the day before implantation and the mice are returned to its home cage for food and water.

For the New Zealand rabbit, after the rabbit ear hair is removed, the skin is disinfected and wiped with alcohol and the auricular vein near the heart is compressed; FOPECs are inserted into the auricular vein at a 30° angle and extended forward by ~0.3 cm, and then they are fixed with medical tape to detect the signal in real time. For specific probe implantation location and section, please refer to table S4 and fig. S21.

Optical setup for sensing

The optical setup for monitoring neurochemical dynamics in vitro is shown in fig. S5. The two fiber-coupled output lasers (central wavelengths are 473 and 561 nm) are coupled into the MMF (core/cladding 200/220 μm, NA 0.37, Inper) and connected with our self-made FOPECs through ceramic sleeves. The fluorescence is collected and guided into the beam splitter [FMC5_E1(460–490) _F1(500–540) _E2(555–570) _F2(580–680) _S, Doric] through the MMF. The beam splitter has two output ports: F1 outputs green fluorescence, and F2 outputs red fluorescence. The fluorescence signals are then converted into electrical signals by two APD modules (C12702-11, Hamamatsu). To obtain a low-noise signal, we use a lock-in amplifier (HF2LI, Zurich Instruments) to modulate the lasers. The 473-nm laser is modulated at 561 Hz, and the 561-nm laser is modulated at 799 Hz. The lock-in amplifier has two digital input/output interfaces (DIO1 and DIO2) for digitalized fluorescence signals from APD modules. A low-pass filter (the order is 4, and the integration time is set to 100 ms) filters out the high-frequency noise to obtain amplified fluorescence signals.

For optimization details about the fabrication of FOPECs, the fluorescence collection efficiency of FOPECs, the process of characterizing the performance of FOPECs in vitro, the process of in vivo detection of neurotransmitter changes in animal brains and blood, the process of EEG recording of mouse epilepsy, the process of viral expression of $GRAB_{NE}$ sensors and detection of NE signals in mice, and cell viability of FOPECs in vitro and in vivo, please refer to Supplementary Text. The methods for detecting neurotransmitters as described in the figures are listed in table S5.

Morphological identification and immunofluorescence examination

To verify the proper placement of the optical fibers (fig. S21), animals are deeply anesthetized and transcardially perfused with 0.1 M PBS, followed by 4% paraformaldehyde-borate fixative (pH 7.4) for 20 min. Brains are removed and then postfixed in the same fixative overnight at 4°C, followed by cryoprotection in 10, 20, and 30% sucrose solution at 4°C before being processed for immunocytochemistry. Brains are sliced into 35-μm sections with a cryostat microtome (CM3050 S, Leica). The sections are collected into four serially ordered sets of sections in PBS. For histology examination, the brain sections are washed in PBS and coverslipped with VECTASHIELD mounting medium containing 4′,6-diamidino-2-phenylindole (F6057, Sigma-Aldrich). To verify the inflammatory response (fig. S13), after an initial blocking step (3% normal donkey serum in 0.01 M PBS containing 1% Triton X-100), the sections are incubated with the following primary antibodies for 24 hours at 4°C: rabbit anti-NeuN (1:1000; ab177487, Abcam) and mouse anti-SOX9 (1:1000; ab76997, Abcam). The sections are washed and incubated with Alexa Fluor 647 donkey anti-mouse immunoglobulin G (IgG; 1:1000, ab150107, Abcam) and

Alexa Fluor 555 donkey anti-rabbit IgG (1:1000, ab150062, Abcam) for 2 hours at approximately 25°C. The fluorescence images are captured using a confocal microscope (FV3000, Olympus).

Statistical analysis

All the statistical tests are two-tailed and performed in MATLAB (R2012b). Except where indicated otherwise, all summary data are presented as means ± SEM. Group differences are analyzed using the paired or unpaired Student's *t* test (GraphPad Prism 7, San Diego, CA, USA). Results with *P* values of less than 0.05 are considered statistically significant.

Supplementary Materials

This PDF file includes:

Supplementary Text
Figs. S1 to S21
Tables S1 to S5
References

View/request a protocol for this paper from *Bio-protocol*.

REFERENCES AND NOTES

1. R. Liu, Z. Feng, D. Li, B. Jin, Y. Lan, L. Meng, Recent trends in carbon-based microelectrodes as electrochemical sensors for neurotransmitter detection: A review. *TrAC Trends Anal. Chem.* **148**, 116541 (2022).
2. M. Lakshmanakumar, N. Nesakumar, A. J. Kulandaisamy, J. B. B. Rayappan, Principles and recent developments in optical and electrochemical sensing of dopamine: A comprehensive review. *Measurement* **183**, 109873 (2021).
3. J. Lietsche, I. Imran, J. Klein, Extracellular levels of ATP and acetylcholine during lithium-pilocarpine induced status epilepticus in rats. *Neurosci. Lett.* **611**, 69–73 (2016).
4. A. J. Espay, P. A. LeWitt, H. Kaufmann, Norepinephrine deficiency in Parkinson's disease: The case for noradrenergic enhancement. *Mov. Disord.* **29**, 1710–1719 (2014).
5. J. C. Day, T. J. Kornecook, R. Quirion, Application of in vivo microdialysis to the study of cholinergic systems. *Methods* **23**, 21–39 (2001).
6. S. Greco, W. Danysz, A. Zivkovic, R. Gross, H. Stark, Microdialysate analysis of monoamine neurotransmitters—A versatile and sensitive LC-MS/MS method. *Anal. Chim. Acta* **771**, 65–72 (2013).
7. V. I. Chefer, A. C. Thompson, A. Zapata, T. S. Shippenberg, Overview of brain microdialysis. *Curr. Protoc. Neurosci.* **47**, 7.1.1–7.1.28 (2009).
8. S. Mingote, J. P. C. de Bruin, M. G. P. Feenstra, Noradrenaline and dopamine efflux in the prefrontal cortex in relation to appetitive classical conditioning. *J. Neurosci.* **24**, 2475–2480 (2004).
9. J. Park, B. M. Kile, R. M. Wightman, In vivo voltammetric monitoring of norepinephrine release in the rat ventral bed nucleus of the stria terminalis and anteroventral thalamic nucleus. *Eur. J. Neurosci.* **30**, 2121–2133 (2009).
10. D. Bruns, Detection of transmitter release with carbon fiber electrodes. *Methods* **33**, 312–321 (2004).
11. J. Li, Y. Liu, L. Yuan, B. Zhang, E. S. Bishop, K. Wang, J. Tang, Y. Zheng, W. Xu, S. Niu, L. Beker, T. L. Li, G. Chen, M. Diyaolu, A. L. Thomas, V. Mottini, J. B. H. Tok, J. C. Y. Dunn, B. Cui, S. P. Pasca, Y. Cui, A. Habtezion, X. Chen, Z. Bao, A tissue-like neurotransmitter sensor for the brain and gut. *Nature* **606**, 94–101 (2022).
12. D. L. Robinson, B. J. Venton, M. Heien, R. M. Wightman, Detecting subsecond dopamine release with fast-scan cyclic voltammetry in vivo. *Clin. Chem.* **49**, 1763–1773 (2003).
13. J. Park, P. Takmakov, R. M. Wightman, In vivo comparison of norepinephrine and dopamine release in rat brain by simultaneous measurements with fast-scan cyclic voltammetry. *J. Neurochem.* **119**, 932–944 (2011).
14. C. Zhao, K. M. Cheung, I. Huang, H. Yang, N. Nakatsuka, W. Liu, Y. Cao, T. Man, P. S. Weiss, H. G. Monbouquette, A. M. Andrews, Implantable aptamer–field-effect transistor neuroprobes for in vivo neurotransmitter monitoring. *Sci. Adv.* **7**, eabj7422 (2021).
15. G. Wu, N. Zhang, A. Matarasso, I. Heck, H. Li, W. Lu, J. G. Phaup, M. J. Schneider, Y. Wu, Z. Weng, H. Sun, Z. Gao, X. Zhang, S. G. Sandberg, D. Parvin, E. Seaholm, S. K. Islam, X. Wang, P. E. M. Phillips, D. C. Castro, S. Ding, D. Li, M. R. Bruchas, Y. Zhang, Implantable aptamer-graphene microtransistors for real-time monitoring of neurochemical release in vivo. *Nano Lett.* **22**, 3668–3677 (2022).
16. N. Nakatsuka, K. Yang, J. M. Abendroth, K. M. Cheung, X. Xu, H. Yang, C. Zhao, B. Zhu, Y. S. Rim, Y. Yang, P. S. Weiss, M. N. Stojanovic, A. M. Andrews, Aptamer–field-effect transistors overcome Debye length limitations for small-molecule sensing. *Science* **362**, 319–324 (2018).
17. H. Tang, P. Lin, H. L. W. Chan, F. Yan, Highly sensitive dopamine biosensors based on organic electrochemical transistors. *Biosens. Bioelectron.* **26**, 4559–4563 (2011).
18. S. Casalini, F. Leonardi, T. Cramer, F. Biscarini, Organic field-effect transistor for label-free dopamine sensing. *Org. Electron.* **14**, 156–163 (2013).
19. W. Wang, F. Zhao, M. Li, C. Zhang, Y. Shao, Y. Tian, A SERS optophysiological probe for the real-time mapping and simultaneous determination of the carbonate concentration and pH value in a live mouse brain. *Angew. Chem. Int. Ed.* **58**, 5256–5260 (2019).
20. A. Muller, V. Joseph, P. A. Slesinger, D. Kleinfeld, Cell-based reporters reveal in vivo dynamics of dopamine and norepinephrine release in murine cortex. *Nat. Methods* **11**, 1245–1252 (2014).
21. Q. Nguyen, L. F. Schroeder, M. Mank, A. Muller, P. Taylor, O. Griesbeck, D. Kleinfeld, An in vivo biosensor for neurotransmitter release and in situ receptor activity. *Nat. Neurosci.* **13**, 127–132 (2010).
22. J. Feng, C. Zhang, J. E. Lischinsky, M. Jing, J. Zhou, H. Wang, Y. Zhang, A. Dong, Z. Wu, H. Wu, W. Chen, P. Zhang, J. Zou, S. A. Hires, J. Zhu, G. Cui, D. Lin, J. Du, Y. Li, A genetically encoded fluorescent sensor for rapid and specific in vivo detection of norepinephrine. *Neuron* **102**, 745–761.e8 (2019).
23. A. Dong, K. He, B. Dudok, J. S. Farrell, W. Guan, D. J. Liput, H. L. Puhl, R. Cai, H. Wang, J. Duan, E. Albarran, J. Ding, D. M. Lovinger, B. Li, I. Soltesz, Y. Li, A fluorescent sensor for spatiotemporally resolved imaging of endocannabinoid dynamics in vivo. *Nat. Biotechnol.* **40**, 787–798 (2022).
24. F. Sun, J. Zhou, B. Dai, T. Qian, J. Zeng, X. Li, Y. Zhuo, Y. Zhang, Y. Wang, C. Qian, K. Tan, J. Feng, H. Dong, D. Lin, G. Cui, Y. Li, Next-generation GRAB sensors for monitoring dopaminergic activity in vivo. *Nat. Methods* **17**, 1156–1166 (2020).
25. J. S. Farrell, R. Colangeli, A. Dong, A. G. George, K. Addo-Osafo, P. J. Kingsley, M. Morena, M. D. Wolff, B. Dudok, K. He, T. A. Patrick, K. A. Sharkey, S. Patel, L. J. Marnett, M. N. Hill, Y. Li, G. C. Teskey, I. Soltesz, In vivo endocannabinoid dynamics at the timescale of physiological and pathological neural activity. *Neuron* **109**, 2398–2403.e4 (2021).
26. T. Patriarchi, J. R. Cho, K. Merten, M. W. Howe, A. Marley, W. Xiong, R. W. Folk, G. J. Broussard, R. Liang, M. J. Jang, H. Zhong, D. Dombeck, M. von Zastrow, A. Nimmerjahn, V. Gradinaru, J. T. Williams, L. Tian, Ultrafast neuronal imaging of dopamine dynamics with designed genetically encoded sensors. *Science* **360**, eaat4422 (2018).
27. C. Dong, Y. Zheng, K. Long-Iyer, E. C. Wright, Y. Li, L. Tian, Fluorescence imaging of neural activity, neurochemical dynamics, and drug-specific receptor conformation with genetically encoded sensors. *Annu. Rev. Neurosci.* **45**, 273–294 (2022).
28. S. Ren, Y. Wang, F. Yue, X. Cheng, R. Dang, Q. Qiao, X. Sun, X. Li, Q. Jiang, J. Yao, H. Qin, G. Wang, X. Liao, D. Gao, J. Xia, J. Zhang, B. Hu, J. Yan, Y. Wang, M. Xu, Y. Han, X. Tang, X. Chen, C. He, Z. Hu, The paraventricular thalamus is a critical thalamic area for wakefulness. *Science* **362**, 429–434 (2018).
29. S. Wu, Z. Liao, J. D. Rizak, N. Zheng, L. Zhang, H. Tang, X. He, Y. Wu, X. He, M. Yang, Z. Li, D. Qin, X. Hu, Comparative study of the transfection efficiency of commonly used viral vectors in rhesus monkey (*Macaca mulatta*) brains. *Zool. Res.* **38**, 88–95 (2017).
30. A. G. Lee, C. P. Arena, D. J. Beebe, S. P. Palecek, Development of macroporous poly(ethylene glycol) hydrogel arrays within microfluidic channels. *Biomacromolecules* **11**, 3316–3324 (2010).
31. X. Liu, T. Tang, E. Tham, H. Yuk, S. Lin, T. K. Lu, X. Zhao, Stretchable living materials and devices with hydrogel-elastomer hybrids hosting programmed cells. *Proc. Natl. Acad. Sci. U.S.A.* **114**, 2200–2205 (2017).
32. M. Anguiano, C. Castilla, M. Maska, C. Ederra, R. Pelaez, X. Morales, G. Munoz-Arrieta, M. Mujika, M. Kozubek, A. Munoz-Barrutia, A. Rouzaut, S. Arana, J. Manuel Garcia-Aznar, C. Ortiz-de-Solorzano, Characterization of three-dimensional cancer cell migration in mixed collagen-Matrigel scaffolds using microfluidics and image analysis. *PLOS ONE* **12**, e0171417 (2017).
33. C. W. Berridge, B. E. Schmeichel, R. A. Espana, Noradrenergic modulation of wakefulness/arousal. *Sleep Med. Rev.* **16**, 187–197 (2012).
34. C. W. Berridge, R. C. Spencer, Differential cognitive actions of norepinephrine a2 and a1 receptor signaling in the prefrontal cortex. *Brain Res.* **1641**, 189–196 (2016).
35. K. Pacak, M. Palkovits, I. J. Kopin, D. S. Goldstein, Stress-induced norepinephrine release in the hypothalamic paraventricular nucleus and pituitary-adrenocortical and sympathoadrenal activity: In vivo microdialysis studies. *Front. Neuroendocrinol.* **16**, 89–150 (1995).
36. P. Campus, V. Colelli, C. Orsini, D. Sarra, S. Cabib, Evidence for the involvement of extinction-associated inhibitory learning in the forced swimming test. *Behav. Brain Res.* **278**, 348–355 (2015).
37. Y. Chandramohan, S. K. Droste, J. S. C. Arthur, J. M. H. M. Reul, The forced swimming-induced behavioural immobility response involves histone H3 phospho-acetylation and c-

Fos induction in dentate gyrus granule neurons via activation of the N-methyl-D-aspartate/extracellular signal-regulated kinase/mitogen- and stress-activated kinase signalling pathway. *Eur. J. Neurosci.* **27**, 2701–2713 (2008).
38. A. Nieoullon, Dopamine and the regulation of cognition and attention. *Prog. Neurobiol.* **67**, 53–83 (2002).
39. O. D. Howes, S. Kapur, The dopamine hypothesis of schizophrenia: Version III—The final common pathway. *Schizophr. Bull.* **35**, 549–562 (2009).
40. J. Jankovic, Parkinson's disease: Clinical features and diagnosis. *J. Neurol. Neurosurg. Psychiatry* **79**, 368–376 (2008).
41. J. Dorszewska, M. Prendecki, M. Lianeri, W. Kozubski, Molecular effects of L-dopa therapy in Parkinson's disease. *Curr. Genomics* **15**, 11–17 (2014).
42. G. M. Everett, J. W. Borcherding, L-dopa: Effect on concentrations of dopamine, norepinephrine, and serotonin in brains of mice. *Science* **168**, 849–850 (1970).
43. A. Marburger, R. Sohr, T. Reum, R. Morgenstern, Comparison by microdialysis of striatal L-DOPA after its systemic administration in rats with probes implanted acutely or through a guide cannula. *J. Neurosci. Methods* **102**, 127–132 (2000).
44. Z. Wu, K. He, Y. Chen, H. Li, S. Pan, B. Li, T. Liu, H. Wang, J. Du, M. Jing, Y. Li, A sensitive GRAB sensor for detecting extracellular ATP in vitro and in vivo. *Neuron* **110**, 770–782.e5 (2022).
45. G. Burnstock, Purinergic nerves. *Pharmacol. Rev.* **24**, 509–581 (1972).
46. F. Dona, I. M. Conceicao, H. Ulrich, E. B. Ribeiro, T. A. Freitas, A. L. Abrahao Nencioni, M. J. da Silva Fernandes, Variations of ATP and its metabolites in the hippocampus of rats subjected to pilocarpine-induced temporal lobe epilepsy. *Purinergic Signal.* **12**, 295–302 (2016).
47. J. V. Nadler, Kainic acid as a tool for the study of temporal lobe epilepsy. *Life Sci.* **29**, 2031–2042 (1981).
48. E. Beamer, G. Conte, T. Engel, ATP release during seizures—A critical evaluation of the evidence. *Brain Res. Bull.* **151**, 65–73 (2019).
49. R. C. Lin, N. H. Neff, S. H. Ngai, E. Costa, Turnover rates of serotonin and norepinephrine in brain of normal and pargyline-treated rats. *Life Sci.* **8**, 1077–1084 (1969).
50. A. Sridharan, S. D. Rajan, J. Muthuswamy, Long-term changes in the material properties of brain tissue at the implant-tissue interface. *J. Neural Eng.* **10**, 066001 (2013).
51. K. Zhou, Y. Lai, X. Chen, K. Sugden, L. Zhang, I. Bennion, A refractometer based on a micro-slot in a fiber Bragg grating formed by chemically assisted femtosecond laser processing. *Opt. Express* **15**, 15848–15853 (2007).
52. M. Choi, J. Choi, S. Kim, S. Nizamoglu, S. Hahn, S. Yun, Light-guiding hydrogels for cell-based sensing and optogenetic synthesis in vivo. *Nat. Photonics* **7**, 987–994 (2013).
53. A. Farrukh, J. I. Paez, A. del Campo, 4D Biomaterials for light-guided angiogenesis. *Adv. Funct. Mater.* **29**, 1807734 (2019).
54. C. S. Hughes, L. M. Postovit, G. A. Lajoie, Matrigel: A complex protein mixture required for optimal growth of cell culture. *Proteomics* **10**, 1886–1890 (2010).
55. D. C. S. Tai, D. A. Hooks, J. D. Harvey, B. H. Smaill, C. Soeller, Illumination and fluorescence collection volumes for fiber optic probes in tissue. *J. Biomed. Opt.* **12**, 034033 (2007).

Acknowledgments: We acknowledge the staff in the laboratory of Y.L. for providing the plasmids needed for the experiments. We thank X. Zhang, Y. Lin, and X. Dong in the laboratory of S.S. for experimental help. **Funding:** This work was supported by the National Natural Science Foundation of China (NSFC) (nos. 32021002 and 61831014) and Tsinghua University Initiative Scientific Research Program (no. 20193080076). **Author contributions:** L.K. conceived the idea of and supervised this project. B.Z., K.F., and J.G. performed the experiments and analyzed data. J.F. and Y.L. provided the biomaterials and helpful discussions. S.S. provided the work conditions for cell culture and helpful discussions. B.Z., K.F., J.G., C.Y., and L.K. drafted the manuscript. All authors critically reviewed and approved the final version of the manuscript. **Competing interests:** L.K., B.Z., and S.S. have pending patent applications on the presented methods filed at the China National Intellectual Property Administration (CN202210181582.2; filed on 25 February 2022). The other authors declare no competing interests. **Data and materials availability:** All data needed to evaluate the conclusions in the paper are present in the paper and/or the Supplementary Materials.

Submitted 28 November 2022
Accepted 27 April 2023
Published 2 June 2023
10.1126/sciadv.adg0218